Journal of Asian Earth Sciences 76 (2013) 1–11

Contents lists available at ScienceDirect

Journal of Asian Earth Sciences

journal homepage: www.elsevier.com/locate/jseaes

Chalcophile element constraints on magma differentiation of Quaternary volcanoes in Tengchong, SW China

Xiao-Wen Huang [a,b], Mei-Fu Zhou [a,c], Christina Yan Wang [d], Paul T. Robinson [c], Jun-Hong Zhao [e], Liang Qi [a,*]

[a] State Key Laboratory of Ore Deposit Geochemistry, Institute of Geochemistry, Chinese Academy of Sciences, Guiyang 550002, China
[b] University of Chinese Academy of Sciences, Beijing 100049, China
[c] Department of Earth Sciences, The University of Hong Kong, Hong Kong, China
[d] Guangzhou Institute of Geochemistry, Chinese Academy of Sciences, Guangzhou 510640, China
[e] State Key Laboratory of Geological Processes and Mineral Resources, China University of Geosciences, Wuhan 430074, China

ARTICLE INFO

Article history:
Received 7 March 2013
Received in revised form 21 June 2013
Accepted 15 July 2013
Available online 23 July 2013

Keywords:
Arc-like volcanic rocks
Platinum-group elements
Magma chamber processes
Tengchong
SW China

ABSTRACT

The Tengchong volcanic field comprises numerous Quaternary volcanoes in SW China. The volcanic rocks are grouped into Units 1–4 from the oldest to youngest. Units 1, 3 and 4 are composed of trachybasalt, basaltic trachyandesite and trachyandesite, respectively, and Unit 2 consists of hornblende-bearing dacite. This rock assemblage resembles those of arc volcanic sequences related to oceanic slab subduction. Rocks of Units 1 and 3 contain olivine phenocrysts with Fo contents ranging from 65 to 85 mole%, indicating early fractionation of olivine and chromite prior to the eruption of magma. All the rocks from Units 1, 3 and 4 have very low PGE concentrations, with <0.05 ppb Ru and Rh, <0.2 ppb Pt and Pd, and Ir that is commonly close to, or slightly higher than detection limits (0.001 ppb). The small variations of Pt/Pd ratios (0.4–2.2) are explained by fractionation of silicate and oxide minerals. The 5-fold variations in Cu/Pd ratios (200,000–1,000,000) for the lavas at Tengchong, which do not vary systematically with fractionation, likely reflect retention of variable amounts of residual sulfide in the mantle source. In addition, all the rocks from Units 1, 3 and 4 have primitive mantle-normalized chalcophile element patterns depleted in PGE relative to Cu. Together with very low Cu/Zr ratios (0.06–0.24), these rocks are considered to have undergone variable degrees of sulfide-saturated differentiation in shallow crustal staging magma chambers. Large amounts of olivine and chromite crystallization probably triggered sulfide saturation of magma at depth for Units 1 and 3, whereas crustal contamination was responsible for sulfide saturation during ascent of magma for Unit 4.

1. Introduction

Widespread volcanic eruptions occurred along the southeastern margin of the Tibetan plateau. Two major volcanic fields include Wuntho, Central Burma and Tengchong, western Yunnan, SW China (Fig. 1). Pliocene to Recent lavas in the Tengchong area of SW China include trachybasalt, basaltic trachyandesite, trachyandesite and dacite that were erupted in four stages. These lavas have arc-like geochemical affinities and have undergone crustal contamination and fractional crystallization prior to eruption (Zhou et al., 2012).

Chalcophile elements, such as Ni and Cu, and platinum-group elements (PGE) can be used to investigate the origin and evolution of mafic-ultramafic rocks, particularly the processes of sulfide saturation and mineral fractionation (e.g. Barnes et al., 1985; Zhou et al., 1998; Philipp et al., 2001; Momme et al., 2003; Wang et al., 2007a, 2011; Qi et al., 2008; Qi and Zhou, 2008; Yang et al., 2011). However, there are only sparse PGE data for intermediate rocks (e.g., Setiabudi et al., 2007; Park et al., 2013). No PGE data are currently available for the Tengchong rocks and their sulfide saturation history and magmatic evolution remain unclear, mainly because of the difficulty in analyzing basaltic/andesitic rocks with very low PGE. The development of a modified digestion method for PGE (Qi et al., 2011) and the application of high-sensitivity ICP-MS, such as that provided by the Bruker Aurora M90, make determination of low-level PGE in Tengchong lavas possible.

Zhou et al. (2012) briefly summarized the petrography and presented detailed major and trace element and isotopic data for the trachybasalt, basaltic trachyandesite, and trachyandesite that comprise Units 1, 3 and 4, respectively. The dacites of Unit 2, which are thought to geochemically independent of the other rocks (Zhou et al., 2012) and are not discussed here. Based on that study, the current paper provides systematic descriptions of the

* Corresponding author. Tel.: +86 851 5891769.
E-mail address: qilianghku@hotmail.com (L. Qi).

1367-9120/$ - see front matter © 2013 Elsevier Ltd. All rights reserved.
http://dx.doi.org/10.1016/j.jseaes.2013.07.020

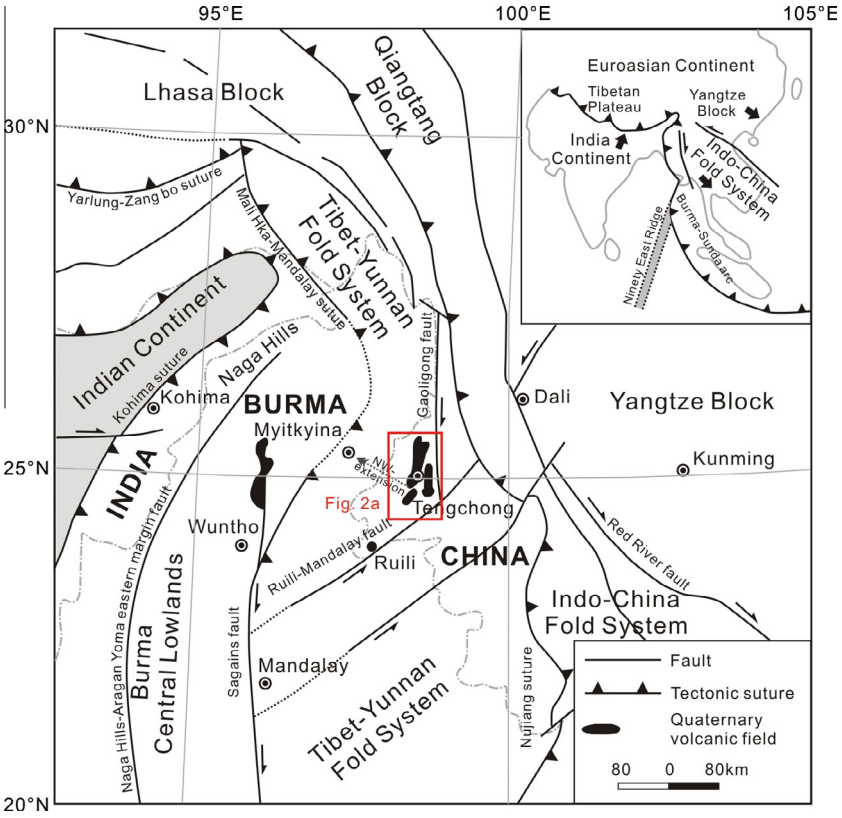

Fig. 1. (a) A simplified geological map showing major tectonic units in a collisional zone between the Indian and Eurasian plates (after Tapponnier et al., 1982; McCaffrey, 2009).

lavas and presents new data sets of olivine compositions and whole-rock chalcophile element concentrations. These new data sets enable us to constrain magma differentiation processes involving both sulfide and silicate fractionation in the magma chamber before eruption of the volcanoes.

2. Geological background

The Tengchong volcanic field lies to the southeast of the Tibetan Plateau. In this region, there are Indian continent, Tibet-Yunnan Fold System, Indo-China Fold System and Yangtze Block from west to east, all of which are separated by regional faults (Fig. 1) (Yan et al., 2006). Sinistral strike-slip motion along the major faults in the region accommodated southeastward escape of the Tibetan Plateau that began at ~27 Ma (Tapponnier et al., 1982; Socquet and Pubellier, 2005) and continues to the present time. The Tibet-Yunnan Fold System is separated from the Yangtze Block by the Red-River fault to the east and from the Burma Central Lowlands to the west by the Mali Hka-Mandalay suture (Fig. 1) (Yan et al., 2006).

The Tengchong volcanic field in the Tibet-Yunnan Fold System is located within pull-apart basins produced in a stress field of NNE-NE-compression and NWW-NW-extension (Wang et al., 2007b) (Fig. 1). The volcanoes occur along the Gaoligong dextral-strike-slip fault near its intersection with the Ruili-Mandalay sinistral strike-slip fault (Fig. 1).

The Tengchong volcanic field, which is ~90 km long from north to south and ~30 km wide (Fig. 2a), includes more than 90 individual cones (Liu, 1999). Mafic-intermediate lavas commonly form stubby flows, up to about 35 m thick, which typically show well-developed columnar jointing (Fig. 3a and b). These flows comprise four principal lithologic units (Fig. 2b). The poorly exposed Unit 1 is only distributed along the Longchuan River (Fig. 2b). Unit 3 is located at the two sides of the Longchuan River and is covered by Unit 4. To the south, Unit 2 in the Yujudashan Mountain is commonly overlain by Quaternary deposits (Fig. 2b). Unit 1, generally considered the oldest, consists of olivine trachybasalt and minor basaltic trachyandesite, whereas a distinct sequence of hornblende dacite makes up Unit 2 (YBGMR, 1979). Relatively uniform basaltic trachyandesite comprises Unit 3, whereas Unit 4, the youngest, consists of siliceous trachyandesite (YBGMR, 1979).

3. Petrography

3.1. Unit 1

Lavas from Unit 1 are fine-grained, moderately phyric, very sparsely vesicular, olivine trachybasalt (Fig. 3c). Phenocrysts make up 10–15 modal% and consist of olivine, plagioclase and clinopyroxene. A few samples have weakly glomerophyric textures with intergrowths of plagioclase and pyroxene. Olivine phenocrysts make up 6–7 modal% and occur chiefly as subhedral to euhedral crystals, 0.5–5 mm across. A few grains are slightly corroded and have wormy textures. Most of the grains are fresh but some have narrow rims of reddish-yellow iddingsite. Plagioclase phenocrysts make up ~5 modal% and occur as subhedral to euhedral laths up to 7 mm in length (Fig. 3d). Some display normal and oscillatory zoning. Plagioclase phenocrysts are all fresh but a few grains have pitted cores. Sparse clinopyroxene phenocrysts make up ~2 modal% and form subhedral laths ranging from 0.5 to 1 mm in length.

All of the samples contain 1–2 modal% of plagioclase and quartz xenocrysts. The plagioclase xenocrysts occur as anhedral to subhedral laths up to 5 mm long, with fritted margins, some of which are surrounded by clear overgrowth rims. A few of the grains also have

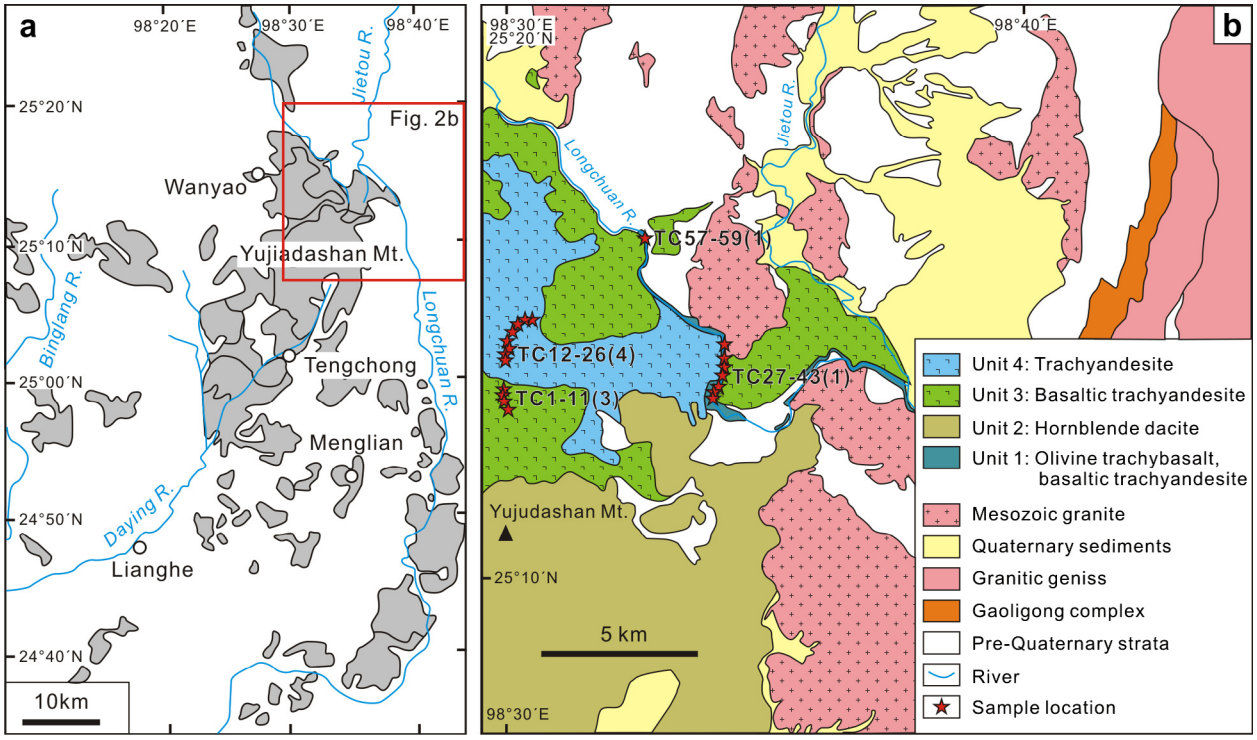

Fig. 2. (a) The distribution of Quaternary volcanic rocks in the Tengchong volcanic field; (b) sampling locations (adapted from an unpublished geological map of 1:50,000 scale by Geological Survey of Yunnan, 2000).

strongly pitted cores. Quartz forms small, subrounded grains, 0.3–0.5 mm across, which are commonly rimmed with clinopyroxene (Fig. 3e).

The groundmass of the olivine trachybasalts is fine-grained and shows intergranular to intersertal, or rarely, subophitic textures (Fig. 3c). It consists chiefly of small (0.1–0.3 mm) plagioclase laths (~75 modal%), granular clinopyroxene (~15 modal%), minute Fe–Ti oxide grains (~2 modal%) and interstitial microcrystalline material (~5 modal%). All of the groundmass is very fresh with only traces of carbonate and yellowish-brown clay minerals.

3.2. Unit 3

The lavas of Unit 3 are moderately to highly vesicular, fine-grained, weakly phyric basaltic trachyandesites. Vesicles vary from ~5% to 20% of the rock and range from 0.5 to 3 mm in size. The smallest vesicles are typically circular, whereas the larger ones are ovoid to irregular, commonly elongate parallel to flow directions.

Phenocrysts make up 5–7 modal% and consist chiefly of olivine and plagioclase with trace amounts of clinopyroxene (Fig. 3f). Olivine usually comprises about half of the phenocrysts but in some samples is confined to the groundmass. Most olivine phenocrysts are euhedral, about 1 mm long, and completely fresh. Plagioclase phenocrysts make up 1–5 modal% and occur as subhedral laths generally 0.1–2 mm long. A few grains are somewhat rounded and others have pitted cores. Clinopyroxene makes up <1 modal% and forms small prisms, 0.3–0.5 mm long. Some samples have a few small, corroded Fe–Ti oxide grains up to 0.1 mm across.

All the samples have 1–2 modal% xenocrysts, typically plagioclase and quartz. The plagioclase crystals are subhedral to rounded, up to 3 mm long, and typically have corroded cores and fritted margins. The rounded quartz grains are mostly ~0.5 mm across and are rimmed with clinopyroxene. One sample (TC-6) has numerous clots of fine-grained clinopyroxene, 0.2–0.3 mm across, that were probably originally small quartz xenocrysts.

The groundmass of these rocks ranges from fine- to very fine-grained and is typically intersertal to intergranular (Fig. 3f). Commonly, fine-grained and coarse-grained patches occur in the same specimen. The coarse-grained patches consist of plagioclase laths up to 0.2 mm long, minute grains of clinopyroxene and about 10 modal% of small, euhedral olivine crystals, 0.01–0.02 mm long. Most samples also contain about 5 modal% of minute Fe–Ti oxide grains. These rocks are typically fresh but a few contain 1–2 modal% of yellow clay minerals.

3.3. Unit 4

Rocks of Unit 4 form a distinctive collection of very fine-grained, moderately to weakly porphyritic, trachyandesites with a glassy groundmass. Many of the rocks have relatively large (1–5 mm) irregular to elongate, open cavities, which make up ~5–15% of the rocks. Phenocrysts make up ~5–12 modal% and consist chiefly of clinopyroxene and small amounts of plagioclase. Clinopyroxene phenocrysts average ~7 modal% and consist of small (0.3–1 mm), subhedral to euhedral crystals (Fig. 3g), many of which are twinned and/or show prominent zoning. Other grains are skeletal in form and contain abundant inclusions of brown glass. Most of the pyroxene is augite but some laths of hypersthene are also present and many of these have narrow rims of augite. A few of the larger hypersthene grains have narrow exsolution lamellae of clinopyroxene. Plagioclase phenocrysts make up 3–5 modal% and occur as small, euhedral laths up to 2 mm long. Some of these grains are zoned but most appear to be uniform in composition. Sparse anhedral Fe–Ti oxides, up to 0.3 mm across, are scattered through the rocks.

In addition to the phenocrysts, these rocks contain relatively abundant xenocrysts of plagioclase and quartz. The plagioclase xenocrysts are irregular to partially rounded laths, up to ~3 mm long, with distinctive fritted margins (Fig. 3h). These make up 2–3 modal% of most rocks. Quartz xenocrysts are small (0.3–0.5 mm), rounded grains typically rimmed with small crystals of

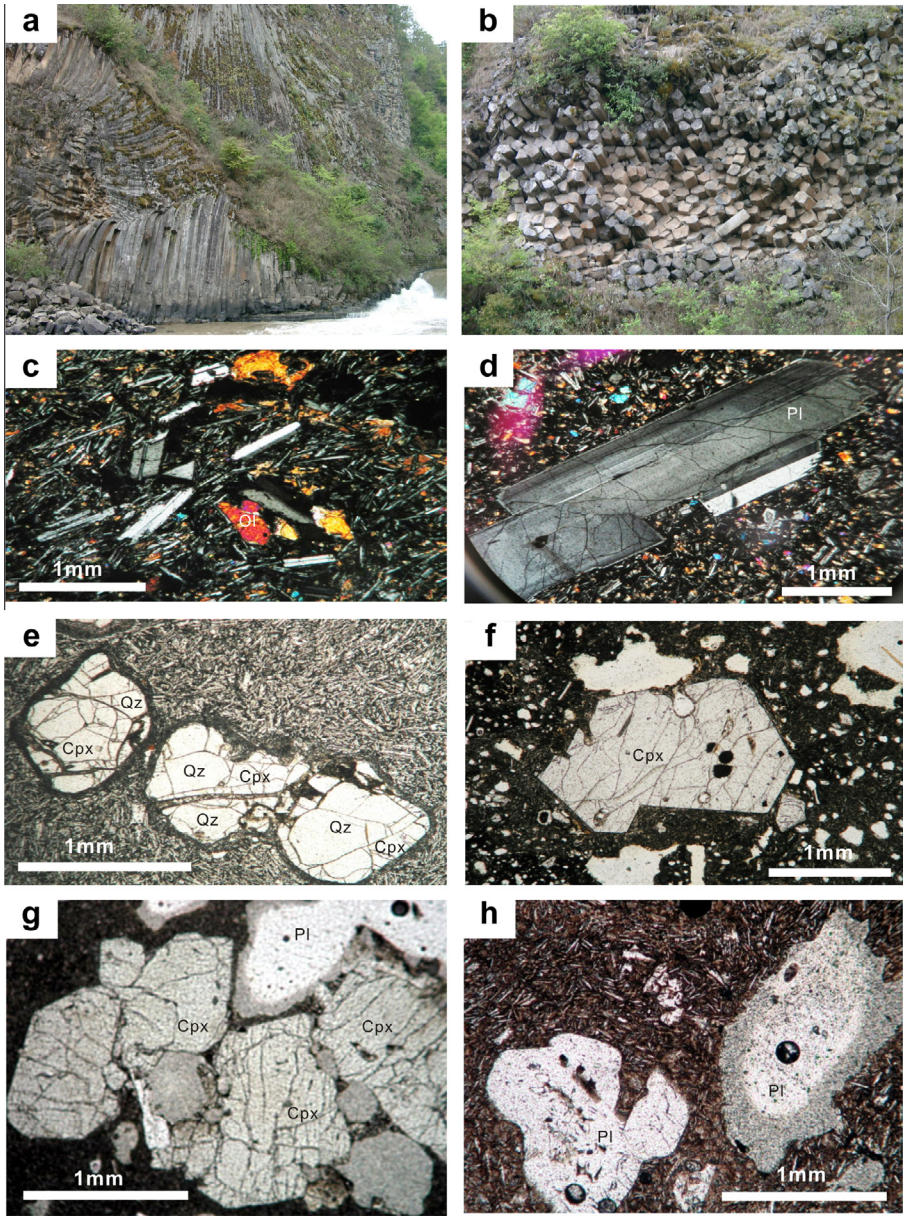

Fig. 3. Field photos (a and b) and photomicrographs (c–h) of the lavas at Tengchong. (a and b) Well-developed columnar jointing of lava flows; (c) olivine trachybasalt of Unit 1 showing interstitial texture (sample TC-34); (d) large, zoned plagioclase phenocryst in trachybasalt of Unit 1 (sample TC-57); (e) quartz xenocrysts with narrow reaction rim of clinopyroxene in trachybasalt of Unit 1 (sample TC-40); (f) euhedral clinopyroxene phenocryst in fine-grained groundmass and abundant small vesicles of basaltic trachyandesite of Unit 3 (sample TC-1); (g) large plagioclase xenocryst with a fritted margin and a cluster of small, subhedral clinopyroxene crystals in porphyritic trachyandesite of Unit 4 (sample TC-25); and (h) large, rounded and fritted xenocrysts of plagioclase and small, euhedral plagioclase laths in the fine-grained, partly devitrified groundmass in trachyandesite of Unit 4 (sample TC-25). Ol-olivine; Cpx-clinopyroxene; Pl-plagioclase; Qz-quartz.

clinopyroxene. Their abundance is highly variable ranging from 1–5 modal%.

The groundmass of these rocks consists chiefly of fresh, brown glass with abundant plagioclase microlites and sparse granular clinopyroxene (Fig. 3h). Some samples show well-developed flow banding and some contain small patches of slightly coarser groundmass material. All of the rocks are very fresh with no observable secondary minerals.

4. Analytical techniques

4.1. Mineral compositions

Major element compositions of minerals were determined with a JEOL JXA-8100 electron microprobe at the Guangzhou Institute of Geochemistry, Chinese Academy of Sciences, using a beam of 15 keV and 10 nA focused to a spot of ~2 μm in diameter. Natural mineral standards were used for calibration and a PAP correction procedure was applied to the data (Pouchou and Pichoir, 1991). The precision of the analyses is better than 5% for major components.

4.2. Whole-rock major and trace elements

Whole-rock major oxides were analyzed by X-ray fluorescence on fused glass beads at the Department of Earth Sciences, the University of Hong Kong, following the analytical procedures of Zhou et al. (2006). Analytical precision is generally better than 1% for SiO_2 and better than 2% for the other oxides. Trace elements were analyzed by inductively coupled plasma-mass spectrometry (ICP-MS) at the Department of Earth Sciences, HKU, according to

Table 1
Blank, detection limits (DL) and analytical results of PGE for standard materials WGB-1, UMT-1 and WPR-1.

Elements (ng/g)	Blank	DL (3σ)	WGB-1		UMT-1		WPR-1	
			Average (1σ, n = 3)	Certified	Average (1σ, n = 3)	Certified	Average (1σ, n = 3)	Certified
Ir	0.002	0.001	0.27 ± 0.03	0.33 ± 0.17	8.23 ± 0.35	8.8 ± 0.6	14.8 ± 1.4	13.5 ± 1.3
Ru	0.002	0.001	0.15 ± 0.02	0.3	9.83 ± 0.82	10.9 ± 1.5	21.2 ± 0.25	21.6 ± 3.3
Rh	0.001	0.001	0.18 ± 0.02	0.32 ± 0.21	8.89 ± 0.6	9.5 ± 1.1	13.7 ± 1.4	13.4 ± 1.6
Pt	0.004	0.003	4.95 ± 0.52	6.1 ± 1.6	135 ± 6	129 ± 5	301 ± 9	285 ± 24
Pd	0.006	0.002	11.8 ± 0.8	13.9 ± 2.1	108 ± 5	106 ± 3	243 ± 9	235 ± 21

Certified = Govindaraju (1994).

Table 2
Representative olivine compositions for lavas from the Tengchong area, SW China.

Sample	TC-29	TC-29	TC-29	TC-29	TC-29	TC-35	TC-36	TC-36	TC-36	TC-36	TC-36	TC-38	TC-29	TC-35	TC-36
Units	1	1	1	1	1	1	1	1	1	1	1	1	1	1	1
Grain	Pheno	Pheno	Pheno	Pheno	Pheno	Pheno	Pheno	Pheno	Pheno	Pheno	Pheno	Pheno	Grdmass	Grdmass	Grdmass
Position	Core	Core	Core	Rim	Core	Core	Core	Rim	Rim	Core	Core	Core	Core	Core	Core
wt%															
SiO_2	39.15	39.56	39.27	40.08	39.65	39.13	39.07	39.28	38.93	39.04	38.89	39.04	36.81	36.67	36.90
Al_2O_3	0.06	0.11	0.02	0.05	0.04	0.11	0.02	0.03	0.05	0.04	0.04	0.04	0.05	0.02	0.04
FeO_t	16.78	15.38	20.35	15.41	15.08	19.60	19.25	17.27	16.27	17.26	16.79	15.43	28.43	29.45	29.25
MnO	0.26	0.21	0.29	0.20	0.20	0.31	0.34	0.30	0.22	0.26	0.25	0.19	0.45	0.47	0.48
MgO	43.08	44.90	39.72	43.25	44.69	39.73	41.60	42.95	43.68	43.09	42.76	43.65	34.41	32.68	33.43
CaO	0.25	0.27	0.26	0.26	0.26	0.20	0.18	0.22	0.24	0.25	0.25	0.22	0.30	0.33	0.48
NiO	0.07	0.11	0.03	0.09	0.15	0.07	0.16	0.12	0.16	0.15	0.17	0.25	0.03	0.08	0.06
Total	99.78	100.73	100.07	99.34	100.07	99.30	100.76	100.18	99.54	100.09	99.14	98.81	100.60	99.70	100.84
Fo	82.1	83.9	77.7	73.7	74.8	78.3	79.4	81.6	72.9	71.4	71.8	73.9	68.3	66.4	67.1
Ni (ppm)	585	853	229	735	1193	585	1248	948	1240	1161	1343	1927	245	652	482

Sample	TC-59	TC-1	TC-1	TC-1	TC-1	TC-10	TC-11	TC-2	TC-5	TC-5	TC-2	TC-5	TC-5	TC-22	TC-22
Units	1	3	3	3	3	3	3	3	3	3	3	3	3	4	4
Grain	Grdmass	Pheno	Pheno	Pheno	Pheno	Pheno	Pheno	Pheno	Pheno	Pheno	Grdmass	Grdmass	Grdmass	Pheno	Pheno
Position	Core	Core	Core	Core	Core	Rim	Core	Core	Core	Core	Core	Core	Core	Core	Rim
wt%															
SiO_2	38.23	39.56	39.41	38.75	40.35	39.55	39.39	35.77	39.73	39.59	36.72	36.66	36.48	38.68	38.07
Al_2O_3	0.05	0.02	0.04	0.07	0.06	0.09	0.03	2.25	0.05	0.01	0.05	0.47	0.00	0.02	0.02
FeO_t	22.50	14.67	15.09	15.33	15.17	15.44	18.30	18.90	15.71	16.06	31.68	34.44	32.01	21.15	24.82
MnO	0.37	0.20	0.23	0.19	0.22	0.25	0.21	0.31	0.20	0.23	0.58	0.54	0.51	0.29	0.38
MgO	38.58	45.85	44.78	44.68	44.36	44.51	42.54	38.14	44.70	44.51	31.28	28.06	30.47	40.10	36.99
CaO	0.20	0.24	0.24	0.22	0.24	0.20	0.21	0.27	0.20	0.21	0.19	0.27	0.21	0.15	0.18
NiO	0.12	0.15	0.12	0.20	0.12	0.19	0.10	0.09	0.20	0.15	0.05	0.11	0.05	0.21	0.10
Total	100.08	100.79	99.90	99.44	100.62	100.29	100.86	95.77	100.80	100.88	100.58	100.63	99.78	100.63	100.63
Fo	75.3	84.8	74.8	74.5	83.9	83.7	80.6	78.2	83.5	83.2	63.8	59.2	62.9	77.2	72.6
Ni (ppm)	980	1177	956	1588	924	1509	782	671	1588	1185	403	885	419	1619	758

Abbreviations: Pheno-Phenocrystal, Grdmass-Groundmass.

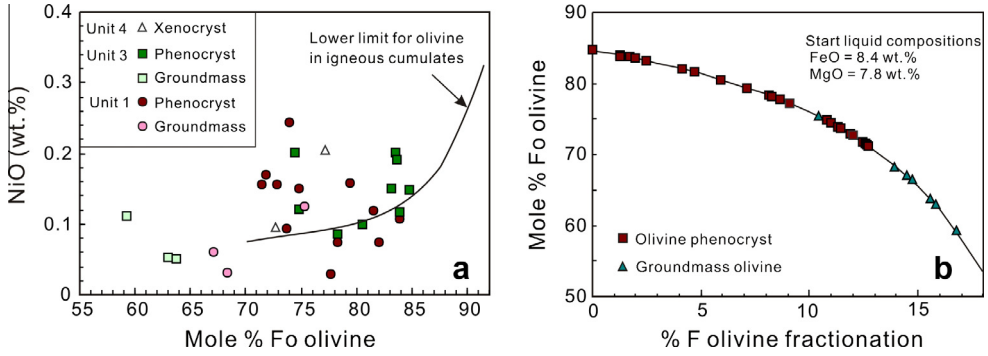

Fig. 4. (a) Plot of Fo versus NiO and (b) Fo versus % F (degree of olivine fractionation) for olivine from the lavas at Tengchong. The lower compositional limit for olivine in igneous cumulates in (a) is from Simkin and Smith (1970). The start liquid compositions are estimated according to the method of Li and Ripley (2011).

procedures described by Qi and Zhou (2008). Analytical precision for most elements is better than 5%.

4.3. Whole-rock platinum group elements

Whole-rock PGE were determined by isotope dilution (ID)-ICP-MS using a modified digestion method (Qi et al., 2011) at the Institute of Geochemistry (Guiyang), Chinese Academy of Sciences. Eight grams of rock powder (>200 mesh) and appropriate amounts of the enriched isotope spike solution ^{101}Ru, ^{193}Ir, ^{105}Pd and ^{194}Pt were weighted and placed in a 120 ml PTFE beaker. About 5 ml of water was added to wet the sample and then 25 ml of HF was added slowly. The solutions were evaporated to dryness to remove silicates. Five ml of HF and 15 ml of HNO_3 were then added. After heating the

sealed bombs at 190 °C for 24 h, the solutions were evaporated to dryness and concentrated HCl was added. After drying, the solutions were conditioned to 2 N HCl and transferred to 50 ml centrifuge tubes. After centrifuging, the supernatant was transferred to the original beaker and used to preconcentrate PGE by Te-coprecipitation. The main interfering elements, such as Cu, Ni, Zr and Hf, were removed by a mixed ion exchange column that contained a Dowex 50 W X8 cation exchange resin and a P507 levextrel resin.

All PGE were determined by a Bruker Aurora M90 ICP-MS. The sensitivity of the instrument was adjusted to more than 1,000,000 cps (counts per second) for 1 ng ml^{-1} of ^{115}In and 300,000 cps for 1 ng ml^{-1} of ^{232}Th using the high sensitivity mode in order to achieve the desired detection limits. The intensity of ^{99}Ru and ^{191}Ir for samples are normally more than 2000 cps and 1000 cps with about 5% of RSD (relative standard deviation) for samples, respectively.

Iridium, Ru, Pt and Pd were measured with isotope dilution and the content of Rh was calculated using ^{194}Pt as an internal standard (Qi et al., 2004). Analytical results for standard reference materials, including WGB-1 (gabbro), WPR-1 (peridotite) and UMT-1 (ultramafic ore tailings), are in good agreement with the certified values (Table 1). The total procedural blanks were lower than 0.002 ng/g for Ru, Rh and Ir, and 0.006 ng/g for Pt and Pd (Table 1). Rocks from Unit 2 contain extremely low PGE, mostly below the detection limits and are not considered further.

5. Analytical results

5.1. Olivine compositions

Olivine occurs both as phenocrysts and in the groundmass of rocks from Units 1 and 3; one olivine xenocryst was found in

Table 3
PGE and trace element compositions of representative lavas from Tengchong, SW China.

Sample	TC-27	TC-28	TC-32	TC-33	TC-35	TC-36	TC-38	TC-40	TC-42	TC-43	TC-57	TC-1	TC-2	TC-5
Units	1	1	1	1	1	1	1	1	1	1	1	3	3	3
MgO (wt%)	5.35	4.44	5.35	5.02	6.19	5.63	5.78	5.76	5.40	5.48	4.84	4.89	5.41	5.33
Mg#	0.50	0.44	0.50	0.49	0.51	0.53	0.53	0.58	0.52	0.52	0.52	0.51	0.53	0.53
PGE (ppb)														
Ir	0.005	0.009	0.003	0.003	0.002	0.005	0.003	0.005	0.003	0.003	0.005	0.003	0.003	0.002
Ru	0.029	0.054	0.017	0.011	0.006	0.019	0.011	0.021	0.007	0.014	0.017	0.026	0.011	0.013
Rh	0.006	0.007	0.003	0.003	0.003	0.009	0.003	0.006	0.002	0.003	0.003	0.006	0.005	0.005
Pt	0.117	0.141	0.060	0.133	0.034	0.108	0.037	0.112	0.065	0.066	0.055	0.089	0.027	0.045
Pd	0.077	0.093	0.042	0.142	0.031	0.167	0.052	0.108	0.069	0.133	0.049	0.024	0.024	0.066
Trace element (ppm)														
Cr	119	71	128	137	38.2	127	132	100	136	139	130	125	131	131
Ni	40.7	39.9	42.9	44.9	45.5	55.4	55.1	78.5	57.5	58.8	44.2	50.6	59.2	59.3
Cu	20.6	23.2	22.3	25.0	34.5	37.1	32.0	26.1	35.4	35.3	25.2	29.4	23.9	29.1
Y	26.7	31.7	28.1	30.0	24.1	23.9	23.1	24.0	24.4	24.5	27.2	25.5	24.9	24.8
Zr	187	218	202	203	142	173	172	210	176	178	241	225	204	202
Nb	24.1	27.7	26.2	25.4	18.4	23.2	22.9	32.6	23.1	23.4	24.0	21.8	23.5	23.5
Ratios														
Pd/Ir	15	10	14	43	15	31	20	22	21	47	10	7	9	27
Pt/Pd	1.5	1.5	1.4	0.9	1.1	0.6	0.7	1.0	0.9	0.5	1.1	3.7	1.2	0.7
Cu/Pd	268,336	250,038	530,551	176,261	1,113,921	221,291	610,698	243,111	514,584	265,848	511,318	1,204,245	1,016,524	438,125
$(Cu/Pd)_{PM}$	38	35	75	25	158	31	87	34	73	38	72	171	144	62
Ni/Cu	2.0	1.7	1.9	1.8	1.3	1.5	1.7	3.0	1.6	1.7	1.8	1.7	2.5	2.0
Cu/Zr	0.11	0.11	0.11	0.12	0.24	0.21	0.19	0.12	0.20	0.20	0.10	0.13	0.12	0.14
Ni/Zr	0.2	0.2	0.2	0.2	0.3	0.3	0.3	0.4	0.3	0.3	0.2	0.2	0.3	0.3

Sample	TC-7	TC-8	TC-9	TC-11	TC-12	TC-14	TC-15	TC-18	TC-19	TC-20	TC-21	TC-24	TC-26
Units	3	3	3	3	4	4	4	4	4	4	4	4	4
MgO (wt%)	5.32	4.88	4.43	4.67	3.48	3.74	3.79	3.63	3.02	3.40	3.70	3.79	3.86
Mg#	0.53	0.53	0.52	0.53	0.51	0.51	0.51	0.51	0.49	0.50	0.51	0.51	0.52
PGE (ppb)													
Ir	0.002	0.004	0.003	0.003	0.005	0.006	0.004	0.004	0.004	0.006	0.006	0.006	0.006
Ru	0.022	0.016	0.012	0.018	0.026	0.026	0.016	0.018	0.017	0.015	0.026	0.015	0.016
Rh	0.008	0.005	0.005	0.007	0.010	0.013	0.018	0.014	0.007	0.016	0.028	0.019	0.023
Pt	0.020	0.061	0.036	0.034	0.066	0.065	0.076	0.091	0.055	0.047	0.062	0.077	0.063
Pd	0.026	0.042	0.029	0.085	0.030	0.031	0.034	0.022	0.029	0.072	0.121	0.052	0.070
Trace element (ppm)													
Cr	135	129	116	119	55.0	52.6	60.0	59.9	52.6	57.6	73.4	59.1	59.8
Ni	61.4	60.2	53.7	54.7	52.5	52.4	57.1	56.2	46.5	55.0	62.8	57.1	57.2
Cu	25.9	30.7	27.9	31.0	22.4	21.5	22.9	23.0	18.3	21.1	25.2	24.1	21.6
Y	26.1	25.5	25.4	25.4	26.7	25.2	25.9	26.7	26.4	27.4	27.6	25.8	25.5
Zr	215	210	206	209	326	320	331	325	304	326	336	323	324
Nb	24.3	23.7	24.1	24.0	29.3	28.2	29.1	28.7	29.5	29.5	30.4	28.6	28.7
Ratios													
Pd/Ir	11	11	8	27	7	6	8	5	7	13	20	8	13
Pt/Pd	0.8	1.5	1.3	0.4	2.2	2.1	2.2	4.1	1.9	0.7	0.5	1.5	0.9
Cu/Pd	992,646	731,910	975,578	365,934	740,285	691,577	670,879	1,027,104	630,168	294,909	209,355	459,589	308,799
$(Cu/Pd)_{PM}$	141	104	138	52	105	98	95	146	89	42	30	65	44
Ni/Cu	2.4	2.0	1.9	1.8	2.3	2.4	2.5	2.4	2.5	2.6	2.5	2.4	2.6
Cu/Zr	0.12	0.15	0.14	0.15	0.07	0.07	0.07	0.07	0.06	0.06	0.08	0.07	0.07
Ni/Zr	0.3	0.3	0.3	0.3	0.2	0.2	0.2	0.2	0.2	0.2	0.2	0.2	0.2

PM-Primitive mantle, normalization values are from Barnes and Maier (1999).

sample TC-22 of Unit 4. The large, zoned olivine phenocrysts (up to 5 mm) in Unit 1 have Fo contents ranging from 84 to 79 mole% (Table 2). Smaller phenocrysts (1–2 mm) are somewhat more iron-rich with Fo values from 78 to 75, whereas the groundmass olivine has Fo values ranging from 68 to 66 (Table 2). Olivine in the lavas of Unit 3 is similar in composition to that in Unit 1. Olivine phenocrysts have Fo values ranging from 85 to 78, whereas olivine grains in groundmass are considerably more Fe-rich with Fo values ranging from 64 to 59 (Table 2 and Fig. 4a). The variation of Fo contents of olivine grains from the three units is consistent with the normal olivine fractionation trend of the magmas (Fig. 4b). Olivine from Units 1 and 3 has NiO contents ranging from 0.03 to 0.24 wt% for phenocrysts, and from 0.03 to 0.12 wt% for that in the groundmass grains (Fig. 4a).

5.2. Whole-rock major and trace elements

The lavas at Tengchong belong to an alkali series (Zhou et al., 2012). Olivine trachybasalts and basaltic trachyandesites from Units 1 and 3 have a relatively narrow range of MgO (4.2 to 6.2 wt%), whereas trachyandesites of Unit 4 have relatively low MgO (3.0 to 3.9 wt%) (Table 3). The samples have variable Cr contents ranging from 38 to 139 ppm and contain 40 to 78 ppm Ni and 18 to 37 ppm Cu, with Ni/Cu ratios ranging from 1 to 3 (Table 3).

5.3. Whole-rock platinum-group elements

All of the rocks from Units 1, 3 and 4 are very poor in PGE, especially Ir, Ru and Rh. Iridium concentrations are commonly close to and/or slightly higher than detection limits (0.001 ppb). The rocks contain <0.05 ppb Ru and Rh, and <0.2 ppb Pt and Pd (Table 3).

There are weakly positive correlations of PGE with MgO for rocks of Unit 4, whereas rocks of Unit 1 show negative correlations of PGE with MgO (Fig. 5a–e). Rocks of Unit 3 show negative correlation of MgO with Ir and Pt (Fig. 5a and d) and poor correlations of MgO with Ru, Rh and Pd (Fig. 5b, c and e).

Iridium shows positive correlations with Ru, Pt and Pd for the rocks of Unit 1 (Fig. 6a–c), whereas rocks of Units 3 and 4 show poor correlations of Ir with Pt and Pd (Fig. 6b and c). Platinum and Pd are correlate positively in rocks of Unit 1 but are poorly correlated in the rocks of Unit 4 (Fig. 6d).

On the primitive mantle-normalized chalcophile element (Ni, PGE and Cu) diagram, all of the rocks have similarly trough-like patterns depleted in PGE relative to Ni and Cu (Fig. 7).

6. Discussion

The Tengchong volcanoes erupted diverse lavas at different stages of their evolution, reflecting several slightly different

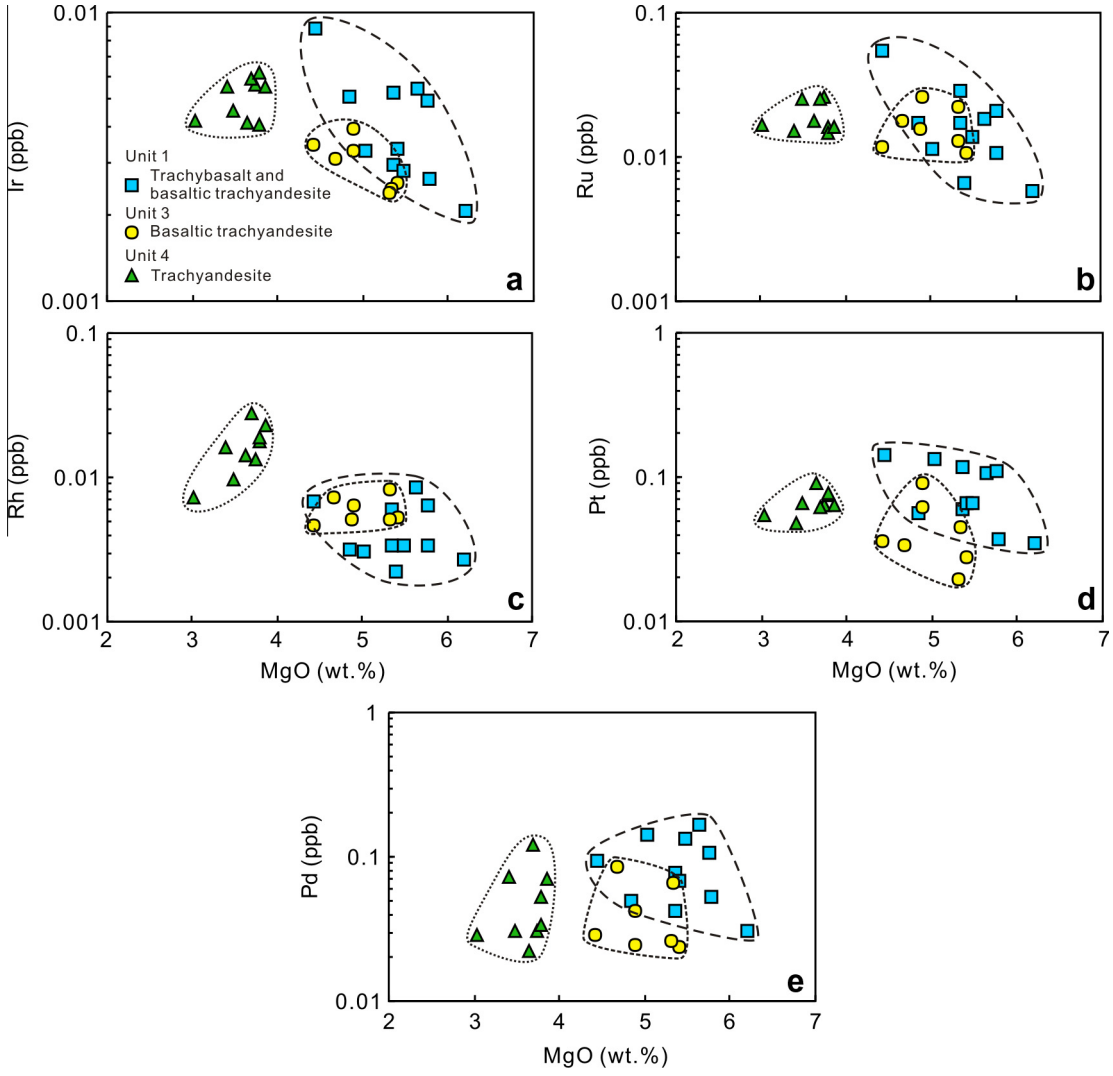

Fig. 5. Plots of PGE versus MgO for the lavas at Tengchong.

parental magmas (Zhou et al., 2012). The lavas at Tengchong are relatively evolved and have experienced fractionation of olivine, plagioclase, pyroxene, apatite and magnetite. Chromite was likely an early crystallizing phase in the magmas that formed Units 1 and 3 (Zhou et al., 2012). All of the Tengchong lavas have very low PGE concentrations (Table 3) and are depleted in PGE relative to Cu and Ni (Fig. 7). The PGE variations together with lithophile element compositions may contain information about the genesis of the magmas and subsequent differentiation processes during magma migration and eruption.

None of the investigated lavas at Tengchong were affected by hydrothermal alteration (Zhou et al., 2012), and hence the PGE of these rocks are not remobilized (Barnes and Liu, 2012). Therefore, we are confident that the reported values of PGE in this study reflect those of the original lavas, and variable PGE concentrations of the lavas can be used to examine the fractionation of olivine and chromite and sulfide saturation history of the magmas.

6.1. Role of olivine and chromite fractionation

Olivine phenocrysts from rocks of Units 1 and 3 have Fo values ranging from 84.8 to 71.2, whereas olivine in the groundmass has Fo values as low as 59.2. The wide range of Fo values for olivine indicates continued crystallization during the migration and eruption of the lavas. Using the MgO–FeO correlation in the lavas and the composition of the most magnesian olivine (Fo = 84.8) from Unit 1, the parental magma from which such olivine crystallized is estimated to have a Mg# of 0.63 and a MgO/FeO ratio of 0.93. In our calculation, we assumed that samples represent olivine-melt mixtures at magmatic temperatures and used the Mg–Fe exchange coefficient of 0.3 between olivine and melt (Roeder and Emslie, 1970). These values are higher than the MgO/FeO ratios of the olivine-bearing Units 1 and 3, indicating significant fractional crystallization before eruption. Using 8.4 wt% FeO and 7.8 wt% MgO as the composition of the parental magma (Li and Ripley, 2011), Units 1 and 3 would have undergone up to 13% fractionation of olivine to produce phenocrysts having compositions of $Fo_{71.2}$ and 17% fractionation to crystallize the groundmass olivine with $Fo_{59.2}$ (Fig. 4b).

The crystallization differentiation of lavas can be judged from the behaviors of incompatible elements such as Nb and Zr and compatible elements such as Cr. The lavas at Tengchong show a positive correlation between Nb and Zr, two elements that are not affected by sulfide fractionation (Fig. 8a). Rocks of Unit 1 with the most abundant phenocrysts composed of olivine, plagioclase and clinopyroxene have low and variable Nb and Zr compared to the rocks of Units 3 and 4 with less phenocrysts (Fig. 8a). The rocks of Units 1 and 3 also have higher Cr and lower Nb than those for the rocks of Unit 4 (Fig. 8b), indicating Cr was compatible during differentiation. In contrast to Cr, Ir is not elevated in the olivine- and chromite-rich samples of Units 1 and 3 and is close to its detection limit (Fig. 8c), indicating that the olivine phenocrysts (with chromite) do not include Ir-bearing alloys or sulfides. Likewise, Pd has a similar variation range in the lavas of the three units (Fig. 8d). Palladium and Ir have comparable silicate melt-sulfide melt partition coefficients (e.g. Fleet et al., 1991; Peach et al., 1994), thus if a suite of lavas undergoes S-saturated differentiation, Pd and Ir would show similarly compatible behaviors. On the other hand, Pd and Ir behave differently during sulfide-undersaturated differentiation because Pd is incompatible but Ir is compatible in olivine or chromite (Barnes et al., 1985). The behavior of Ir and Pd in the lavas at Tengchong indicates that the variation of Pd is not controlled by fractionation of silicate and chromite.

6.2. Role of sulfide fractionation

Both trachybasalt and trachyandesite at Tengchong have very low PGE concentrations, and they show depletion of PGE relative to Ni and Cu on the primitive mantle-normalized chalcophile element patterns (Fig. 7), a feature of sulfide removal/saturation (Barnes et al., 1985; Fleet et al., 1991). Some olivine grains from the Tengchong lavas have ~0.2 wt% NiO at Fo_{84-75}, indicating that these olivines with relatively high Ni contents may have formed before S-saturation. However, most olivine phenocrysts at Tengchong have NiO contents between ~0.1 and ~0.2 wt%, much lower than olivine crystallized from unfractionated, S-undersaturated, high-Mg basaltic melts. For example, olivine from picrites of the

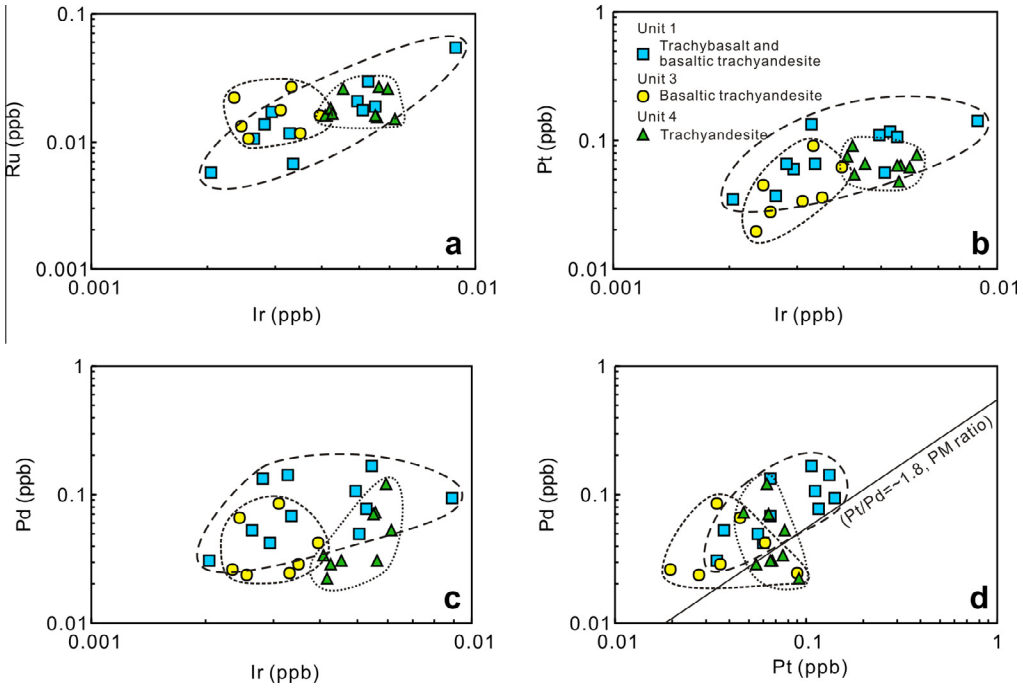

Fig. 6. Plots of Ir versus Ru (a), Ir versus Pt (b), Ir versus Pd (c) and Pt versus Pd (d) for the lavas at Tengchong. Platinum and Pd contents of primitive mantle are after Barnes and Maier (1999).

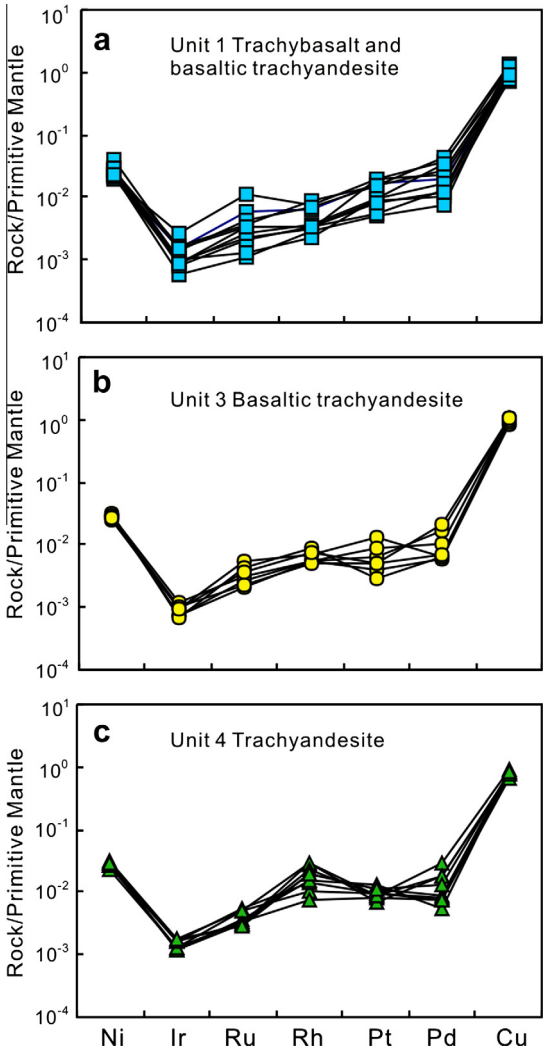

Fig. 7. Primitive mantle-normalized plots of chalcophile elements (Ni, PGE and Cu) for the lavas at Tengchong. Normalization values are after Barnes and Maier (1999).

Emeishan large igneous province has 0.31 wt% NiO at Fo_{84} (Wang et al., 2007a), whereas olivine from Unit 1 at Tengchong with the highest Fo (83.9) has 0.11 wt% NiO, and olivine from Unit 3 with a composition of $Fo_{84.8}$ has 0.15 wt% NiO (Table 2). The low Ni content of olivine is likely indicative of previous sulfide segregation.

Cu/Zr ratio is also a useful indicator of sulfide segregation. Typically, mafic magmas that were not depleted in chalcophile metals have Cu/Zr ratios around 1, whereas magmas that experienced sulfide segregation have Cu/Zr ratios less than unity (Lightfoot and Keays, 2005). The basaltic rocks at Tengchong have somewhat low and variable Cu/Zr ratios (0.06–0.24; Table 3), again indicating removal of sulfide during magma evolution. Moreover, positive correlation of Cu versus Cu/Zr ratios (Fig. 9a) and negative correlation of Zr versus Cu/Zr ratios (Fig. 9b) are consistent with S-saturated fractionation.

However, the lavas at Tengchong show poor correlations of Ir with Ru, Pt and Pd (Fig. 6), indicating that sulfide segregation was not the only control on PGE in the lavas. Pt/Pd ratios of the Tengchong lavas range from 0.4 to 4.1 and most of them are lower than the primitive mantle ratio (~1.8) (Barnes and Maier, 1999) (Fig. 6d), indicating significant fractionation of Pt from Pd. Platinum is more readily fractionated than Pd into oxide phases such as chromite or PGE alloys (e.g. Pt–Fe alloys) under S-undersaturated condition (Momme et al., 2002). Thus, fractionation of S-undersaturated magma would result in more depletion of Pt than Pd. In contrast, Pd has a larger sulfide melt/silicate melt partition coefficient than Pt (Fleet et al., 1991; Peach et al., 1994; Vogel and Keays, 1997) so that Pd would be preferentially removed from S-saturated magma resulting in elevated Pt/Pd ratios in the residual magmas. Lavas at Tengchong have Cu/Pd ratios that do not vary systematically with Pt/Pd ratios (Fig. 10a), indicating sulfide fractionation had little effect on the variations of Pt/Pd ratios. Lavas of Unit 1 have Ni/Zr ratios varying against restricted Pt/Pd ratios, indicating a pure silicate fractionation (Fig. 10b). Poor correlations between Pt/Pd and Ni/Zr ratios of the lavas from Units 3 and 4 (Fig. 10b) indicate that Pt/Pd ratios were not controlled by fractionation of silicate minerals, chromite and even PGE-bearing sulfides. These non-systematic variations of PGE in the lavas of Units 3 and 4 probably reflect the uneven presence of minor sulfides in the lavas.

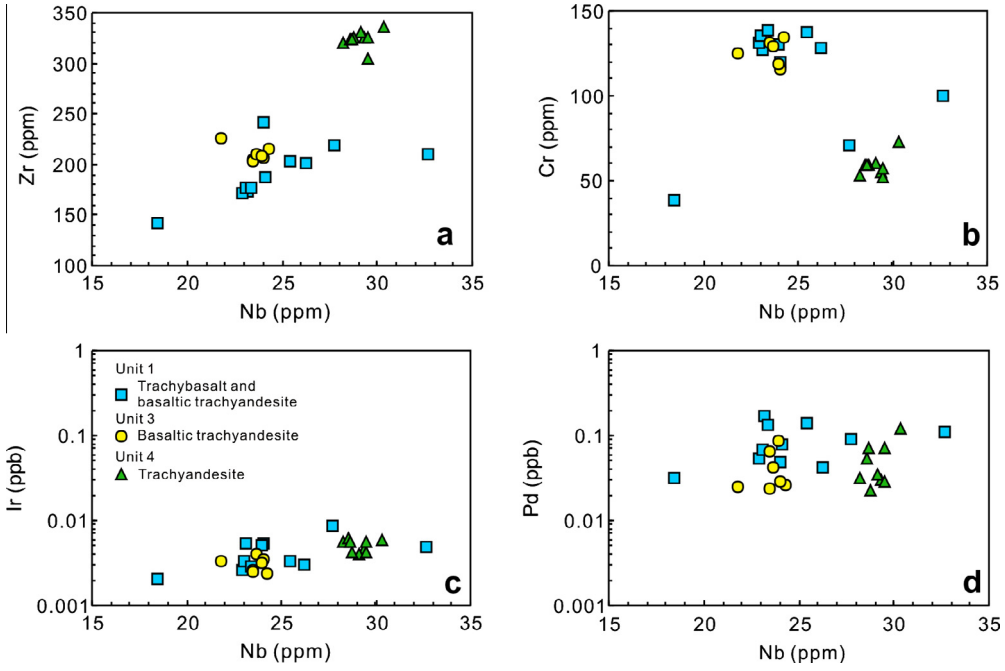

Fig. 8. Plots of Nb versus Zr (a), Cr (b), Ir (c) and Pd (d) for the lavas at Tengchong.

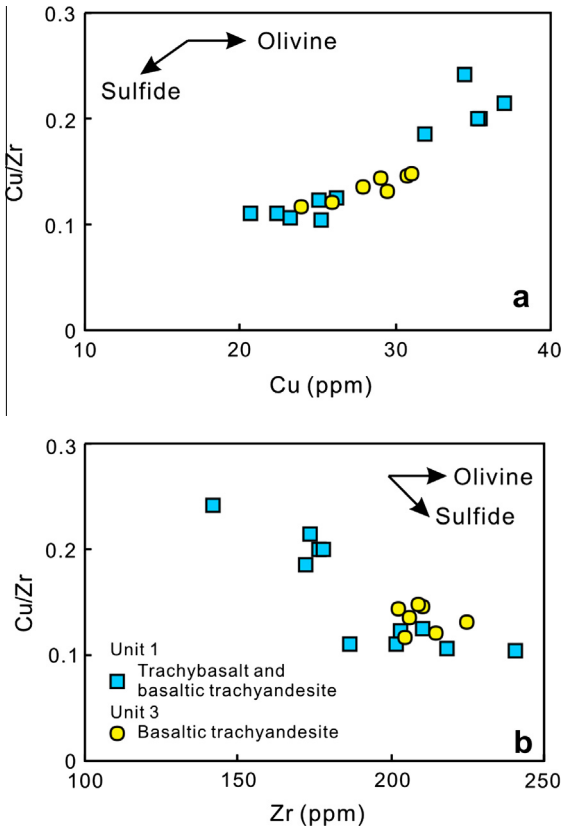

Fig. 9. Plots of Cu and Zr versus Cu/Zr for the lavas at Tengchong.

6.3. Sulfide retention in the mantle source

The low PGE concentrations of the lavas may be caused by sulfide retention in the mantle source or sulfide removal during magma ascent, or both. This can be assessed using the variation of Cu/Pd ratios. Because Pd has a much higher partition coefficient than Cu for sulfide, the resulting magmas after sulfide segregation would have higher Cu/Pd ratios than the mantle value of ~7000 (Barnes and Maier, 1999). On the other hand, mafic rocks with highly variable Cu/Pd ratios may have formed from magmas that experienced sulfide removal at depth (Keays, 1995). All the rocks at Tengchong have very high, variable Cu/Pd ratios from 200,000 to 1,000,000, much higher than the mantle ratio (Fig. 11a). The mantle normalized $(Cu/Pd)_{PM}$ ratios of the Tengchong lavas range from 25 to 170 (Table 3 and Fig. 10a).

Lavas at Tengchong have low Cu and very high Cu/Pd ratios and plot well above arc basalts, Hawaiian picrites and flood basalts of the Siberian Traps (Fig. 11a). Bennett et al. (2000) interpreted the variation of PGE concentrations of Hawaiian picrites to reflect variable amounts or compositions of residual sulfide during partial melting. It is noteworthy that Cu/Pd ratios decrease by a factor of ~18 (Cu/Pd 118,000 to 6400) during the last 1%-step of a batch melting model in which sulfide is exhausted in the mantle and Pd is completely released into the partial melt (Barnes and Maier, 1999). The 5-fold variations in Cu/Pd ratios (200,000–1,000,000) for the Tengchong lavas, which do not vary systematically with fractionation (Fig. 11b), likely reflect retention of variable amounts of residual sulfide in the mantle source. The low PGE of the lavas strongly suggest significant amounts of residual sulfide in the source.

6.4. Sulfide saturation during magma ascent

The very low PGE concentrations of the Tengchong lavas cannot be explained by residual sulfide in the mantle source alone. The flat PGE patterns relative to Cu and Ni (Fig. 7) may indicate that the low PGE concentrations of the lavas can also be attributed to subsequent segregation of sulfide during differentiation (Barnes et al., 1985).

Lavas of Units 1 and 3 experienced early fractionation of olivine and chromite from primitive magmas that would rapidly lower the

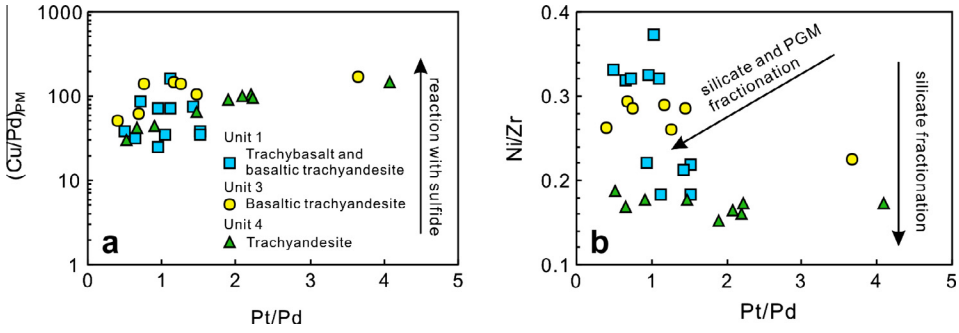

Fig. 10. Plots of Pt/Pd versus $(Cu/Pd)_{PM}$ (a) and Ni/Zr (b) for the lavas at Tengchong.

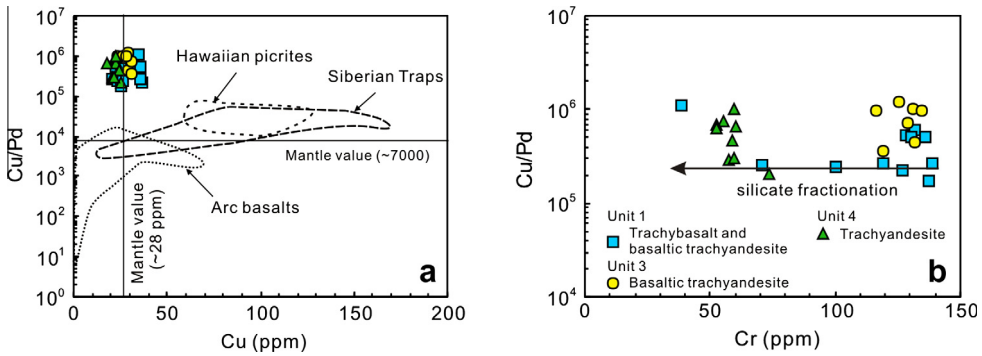

Fig. 11. Plots of Cu versus Cu/Pd ratios (a) and Cr versus Cu/Pd ratios (b) for the lavas at Tengchong. Reference fields in (a) are after Brügmann et al. (1987, 1993), Barnes and Picard (1993) and Bennett et al. (2000).

FeO content in the magma. Therefore, continuous olivine and chromite crystallization probably triggered sulfide saturation of the magma at depth for Units 1 and 3.

Assimilation-induced sulfide saturation has been proposed for continental flood basalts such as the Siberian Traps (Lightfoot and Keays, 2005) and West Greenland (Keays and Lightfoot, 2007). A genetic link between S saturation and crustal contamination was also demonstrated for the low-Ti basalts from the Emeishan large igneous province by negative correlations of Pt and Pd contents with Zr/Nb and Th/Nb ratios (Song et al., 2006, 2009). Lavas of Unit 4 at Tengchong are the most siliceous and have high $^{87}Sr/^{86}Sr$ ratios (~0.7085) and very low εNd values (−8.4 to −8.7) (Zhou et al., 2012). Therefore, sulfide saturation of the Unit 4 lavas was likely triggered by crustal contamination.

7. Conclusions

Lavas at Tengchong include trachybasalts, basaltic trachyandesites, trachyandesites and dacites. All the rocks are poor in PGE due to sulfide retention in the source and sulfide fractionation during magma ascent. Rocks of Units 1 and 3 experienced extensive fractionation of olivine and chromite, which induced sulfide saturation, whereas sulfide saturation for rocks of Unit 4 probably resulted from significant crustal contamination.

Acknowledgments

This study is supported by the Research Grant Council of Hong Kong (HKU706413P) to MFZ. Support from CAS Hundred Talents projects to CYW and LQ, and a CAS/SAFEA International Partnership Program for Creative Research Teams (KZCX2-YW-t004), are gratefully acknowledged. Field assistance was provided by Xu Zhangbao from the Yunnan Geological Survey. We thank Prof. Zhao Taiping and an anonymous reviewer for their constructive reviews.

References

Barnes, S., Liu, W., 2012. Pt and Pd mobility in hydrothermal fluids: evidence from komatiites and from thermodynamic modelling. Ore Geol. Rev. 44, 49–58.

Barnes, S.J., Maier, W.D., 1999. The fractionation of Ni, Cu and the noble metals in silicate and sulphide liquids. In: Keays, R.R., Lesher, C.M. Lightfoot, P.C. Farrow, C.E.G. (Eds.), Dynamic Processes in Magmatic ore Deposits and their Application to Mineral Exploration. Geological Association of Canada, Short Course Notes 13, pp. 69–106.

Barnes, S.J., Picard, C.P., 1993. The behaviour of platinum-group elements during partial melting, crystal fractionation, and sulphide segregation: an example from the Cape Smith Fold Belt, northern Quebec. Geochim. Cosmochim. Acta 57, 79–87.

Barnes, S.J., Naldrett, A.J., Gorton, M.P., 1985. The origin of the fractionation of platinum-group elements in terrestrial magmas. Chem. Geol. 53, 303–323.

Bennett, V.C., Norman, M.D., Garcia, M.O., 2000. Rhenium and platinum group element abundances correlated with mantle source components in Hawaiian picrites: sulphides in the plume. Earth Planet. Sci. Lett. 183, 513–526.

Brügmann, G.E., Arndt, N.T., Hofmann, A.W., Tobschall, H.J., 1987. Noble metal abundances in komatiite suites from Alexo, Ontario and Gorgona Island, Colombia. Geochim. Cosmochim. Acta 51, 2159–2169.

Brügmann, G.E., Naldrett, A.J., Asif, M., Lightfoot, P.C., Gorbachev, N.S., Fedorenko, V.A., 1993. Siderophile and chalcophile metals as tracers of the evolution of the Siberian Trap in the Noril'sk region, Russia. Geochim. Cosmochim. Acta 57, 2001–2018.

Fleet, M.E., Stone, W.E., Crocket, J.H., 1991. Partitioning of palladium, iridium, and platinum between sulfide liquid and basalt melt: effects of melt composition, concentration, and oxygen fugacity. Geochim. Cosmochim. Acta 55, 2545–2554.

Govindaraju, K., 1994. Compilation of working values and sample description for 383 geostandards. Geostandards Newslett. 18, 1–158.

Keays, R.R., 1995. The role of komatiitic and picritic magmatism and S-saturation in the formation of ore deposits. Lithos 34, 1–18.

Keays, R.R., Lightfoot, P.C., 2007. Siderophile and chalcophile metal variations in Tertiary picrites and basalts from West Greenland with implications for the sulphide saturation history of continental flood basalt magmas. Miner. Deposita 42, 319–336.

Li, C., Ripley, E.M., 2011. The giant Jinchuan Ni–Cu-(PGE) deposit: tectonic setting, magma evolution, ore genesis, and exploration implications. In: Li, C., Ripley, E.M. (Eds.), Magmatic Ni–Cu and PGE Deposits: Geology, Geochemistry and Genesis. Society of Economic Geology Special Publication 17, pp. 163–180.

Lightfoot, P.C., Keays, R.R., 2005. Siderophile and chalcophile metal variations in flood basalts from the Siberian Trap, Noril'sk Region: Implications for the origin of the Ni–Cu-PGE sulfide ores. Econ. Geol. 100, 439–462.

Liu, J.Q., 1999. Volcanoes of China. Science Press, Beijing (in Chinese).

McCaffrey, R., 2009. The tectonic framework of the Sumatran subduction zone. Annu. Rev. Earth Planet. Sci. 37, 345–366.

Momme, P., Tegner, C., Brooks, K.C., Keays, R.R., 2002. The behaviour of platinum-group elements in basalts from the East Greenland rifted margin. Contrib. Miner. Petrol. 143, 133–153.

Momme, P., Óskarsson, N., Keays, R.R., 2003. Platinum-group elements in the Icelandic rift system: melting processes and mantle sources beneath Iceland. Chem. Geol. 196, 209–234.

Park, J.-W., Campbell, I.H., Ickert, R.B., Allen, C.M., 2013. Chalcophile element geochemistry of the Boggy Plain zoned pluton, southeastern Australia: a S-saturated barren compositionally diverse magmatic system. Contrib. Miner. Petrol. 165, 217–236.

Peach, C.L., Mathez, E.A., Keays, R.R., Reeves, S.J., 1994. Experimentally determined sulfide melt-silicate melt partition coefficients for iridium and palladium. Chem. Geol. 117, 361–377.

Philipp, H., Eckhardt, J.D., Puchelt, H., 2001. Platinum-group elements (PGE) in basalts of the seaward-dipping reflector sequence, SE Greenland Coast. J. Petrol. 42, 407–432.

Pouchou, J.L., Pichoir, F., 1991. Quantitative analysis of homogeneous or stratified microvolumes applying the model "PAP". In: Heinrich, K.F.J., Newbury, D.E. (Eds.), Electron Probe Quantitation. Plenum Press, New York, pp. 31–75.

Qi, L., Zhou, M.F., 2008. Platinum-group elemental and Sr–Nd–Os isotopic geochemistry of Permian Emeishan flood basalts in Guizhou Province, SW China. Chem. Geol. 248, 83–103.

Qi, L., Zhou, M.-F., Wang, C.Y., 2004. Determination of low concentrations of platinum group elements in geological samples by ID-ICP-MS. J. Anal. At. Spectrom. 19, 1335–1339.

Qi, L., Wang, C.Y., Zhou, M.-F., 2008. Controls on the PGE distribution of Permian Emeishan alkaline and peralkaline volcanic rocks in Longzhoushan, Sichuan Province, SW China. Lithos 106, 222–236.

Qi, L., Gao, J., Huang, X., Hu, J., Zhou, M.-F., Zhong, H., 2011. An improved digestion technique for determination of platinum group elements in geological samples. J. Anal. At. Spectrom. 26, 1900–1904.

Roeder, P.L., Emslie, R.F., 1970. Olivine-liquid equilibrium. Contrib. Miner. Petrol. 29, 275–289.

Setiabudi, B.T., Campbell, I.H., Martin, C.E., Allen, C.M., 2007. Platinum group element geochemistry of andesite intrusions of the Kelian region, East Kalimantan, Indonesia: implications of gold depletion in the intrusions associated with the Kelian gold deposit. Econ. Geol. 102, 95–108.

Simkin, T., Smith, J.V., 1970. Minor-element distribution in olivine. J. Geol. 78, 304–325.

Socquet, A., Pubellier, M., 2005. Cenozoic deformation in western Yunnan (China-Myanmar border). J. Asian Earth Sci. 24, 495–515.

Song, X.Y., Zhou, M.F., Keays, R.R., Cao, Z.M., Sun, M., Qi, L., 2006. Geochemistry of the Emeishan flood basalts at Yangliuping, Sichuan, SW China: implications for sulfide segregation. Contrib. Miner. Petrol. 152, 53–74.

Song, X.Y., Keays, R.R., Xiao, L., Qi, H.W., Ihlenfeld, C., 2009. Platinum-group element geochemistry of the continental flood basalts in the central Emeisihan Large Igneous Province, SW China. Chem. Geol. 262, 246–261.

Tapponnier, P., Peltzer, G., Le Dain, A.Y., Armijo, R., Cobbold, P., 1982. Propagating extrusion tectonics in Asia: new insights from simple experiments with plasticine. Geology 10, 611–616.

Vogel, D.C., Keays, R.R., 1997. The petrogenesis and platinum-group element geochemistry of the Newer Volcanic Province, Victoria, Australia. Chem. Geol. 136, 181–204.

Wang, C.Y., Zhou, M.F., Qi, L., 2007a. Permian flood basalts and mafic intrusions in the Jinping (SW China)-Song Da (northern Vietnam) district: Mantle sources, crustal contamination and sulfide segregation. Chem. Geol. 243, 317–343.

Wang, Y., Zhang, X., Jiang, C., Wei, H., Wan, J., 2007b. Tectonic controls on the late Miocene–Holocene volcanic eruptions of the Tengchong volcanic field along the southeastern margin of the Tibetan plateau. J. Asian Earth Sci. 30, 375–389.

Wang, C.Y., Zhou, M.F., Qi, L., 2011. Chalcophile element geochemistry and petrogenesis of high-Ti and low-Ti magmas in the Permian Emeishan large igneous province, SW China. Contrib. Miner. Petrol. 161, 237–254.

Yan, D.P., Zhou, M.F., Wang, C.Y., Xia, B., 2006. Structural and geochronological constraints on the tectonic evolution of the Dulong-Song Chay tectonic dome in Yunnan province, SW China. J. Asian Earth Sci. 28, 332–353.

Yang, A.Y., Zhao, T.P., Qi, L., Yang, S.H., Zhou, M.F., 2011. Chalcophile elemental constraints on sulfide-saturated fractionation of Cenozoic basalts and andesites in SE China. Lithos 127, 323–335.

YBGMR (Yunnan Bureau of Geology and Mineral Resources). 1979. Techong geologic map (1: 200000) (in Chinese).

Zhou, M.F., Sun, M., Keays, R.R., Kerrich, R.W., 1998. Controls on platinum-group elemental distributions of podiform chromitites: a case study of high-Cr and high-Al chromitites from Chinese orogenic belts. Geochim. Cosmochim. Acta 62, 677–688.

Zhou, M.F., Zhao, J.H., Qi, L., Su, W., Hu, R., 2006. Zircon U–Pb geochronology and elemental and Sr–Nd isotope geochemistry of Permian mafic rocks in the Funing area, SW China. Contrib. Miner. Petrol. 151, 1–19.

Zhou, M.F., Robinson, P.T., Wang, C.Y., Zhao, J.H., Yan, D.P., Gao, J.F., Malpas, J., 2012. Heterogeneous mantle source and magma differentiation of Quaternary arc-like volcanic rocks from Tengchong, SE margin of the Tibetan Plateau. Contrib. Miner. Petrol. 163, 841–860.